Nanoscale Design of Multifunctional Organic Layers for Low-Power High-Density Memory Devices

Laurianne Nougaret,[†] Hailu G. Kassa,[†] Ronggang Cai,[†] Tilia Patois,[†] Bernard Nysten,[†] Albert J. J. M. van Breemen,[‡] Gerwin H. Gelinck,[‡] Dago M. de Leeuw,[§] Alessio Marrani,[⊥] Zhijun Hu,[∥] and Alain M. Jonas[†,*]

[†]Bio & Soft Matter, Institute of Condensed Matter and Nanosciences, Université catholique de Louvain, Croix du Sud 1/L7.04.02, Louvain-la-Neuve 1348, Belgium, [‡]Holst Centre/TNO, High Tech Campus 31, 5656 AE Eindhoven, The Netherlands, [§]Max Planck Institute for Polymer Research, Ackermannweg 10, Mainz 55128, Germany, [⊥]Solvay Specialty Polymers Italy S.P.A., Research and Development Center, Viale Lombardia, No. 20, Bollate MI 20021, Italy, and [∥]Center for Soft Condensed Matter Physics and Interdisciplinary Research, Soochow University, Suzhou 215006, China

ABSTRACT We demonstrate the design of a multifunctional organic layer by the rational combination of nanosized regions of two functional polymers. Instead of relying on a spontaneous and random phase separation process or on the tedious synthesis of block copolymers, the method involves the nanomolding of a first component, followed by the filling of the resulting open spaces by a second component. We apply this methodology to fabricate organic nonvolatile memory diodes of high density. These are built by first creating a regular array of ferroelectric nanodots by nanoimprint lithography, followed by the filling of the trenches separating the ferroelectric nanodots with a semiconducting polymer. The modulation of the current in the semiconductor by the polarization state of the ferroelectric material is demonstrated both at the scale of a single semiconductor channel and in a microscopic device measuring about 80 000 channels in parallel, for voltages below *ca.* 2 V. The fabrication process, which combines synergetically orthogonal functional properties with a fine control over their spatial distribution, is thus demonstrated to be efficient over large areas.

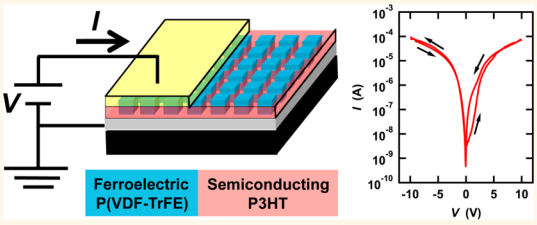

KEYWORDS: organic electronics · ferroelectric polymer · semiconducting polymer · nanoimprint lithography · nonvolatile memory

A rich variety of functional polymer molecules have been synthesized by chemists over the last decades, giving access to properties such as conductivity, semiconductivity, electroluminescence, ferroelectricity, catalysis, *etc*. When a combination of such properties is desired, blending two-component polymers might be an option. However, due to the immiscibility of most polymer molecules, the resulting material usually consists of coarse distributions of regions of large size of the two components.[1] Although sometimes of interest for mechanical properties, such morphologies are limited with respect to functional properties. In this case, the block copolymerization of functional sequences is another option, however, involving considerable synthetic complexity except for the most trivial polymers.[2] In addition, the solid-state microstructure of block copolymers, which consists of regions of 10−100 nm size of various periodicity and shape, remains difficult to control. Here, we demonstrate an alternative route, allowing us to design organic layers consisting of nanoregions of well-defined size and shape, made of two functional polymer components interacting synergetically to provide a new functionality. This is performed by simple operations involving the nanomolding of the first polymer material, followed by the filling of open cavities by a second functional polymer material. Our concept is demonstrated in the context of organic nonvolatile memory devices: we show that ferroelectric memory devices of potentially extremely large density (up to 0.2 Gb/cm^2) can be obtained by the proper rational nanoprocessing of a composite semiconducting/ferroelectric active layer.

Emerging applications of organic electronics such as electronic paper, smart labels, and RFID tags require nonvolatile memories capable of retaining information when power is turned off. Such memories are

* Address correspondence to alain.jonas@uclouvain.be.

Received for review December 19, 2013 and accepted March 20, 2014.

Published online March 20, 2014
10.1021/nn406503g

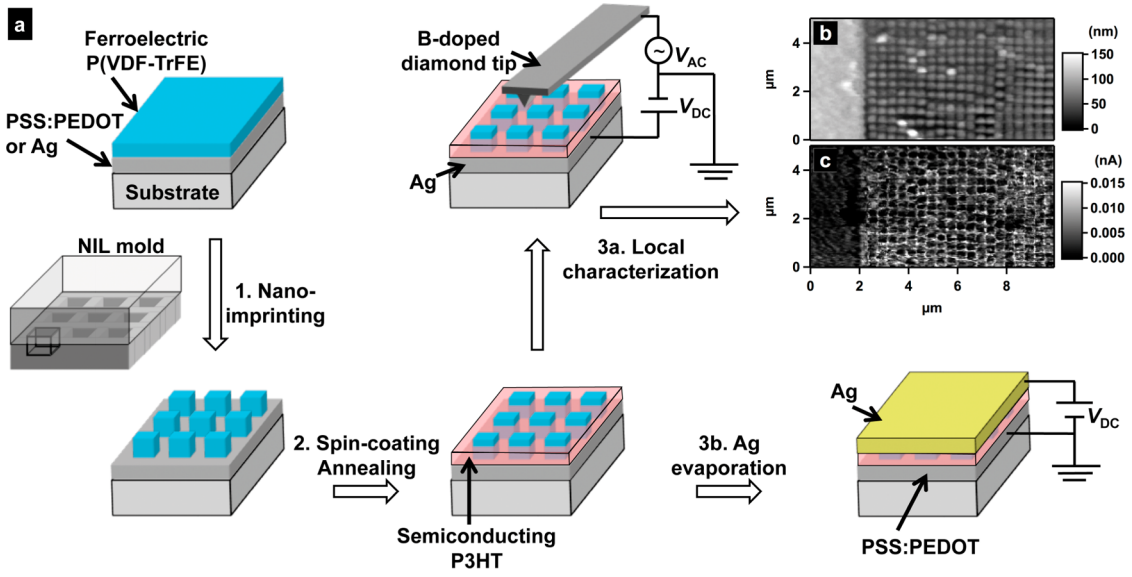

Figure 1. (a) Fabrication process of nanoimprinted ferroelectric/semiconducting memory diodes. Two configurations are used to characterize the diodes (local, path 3a, and in a microscopic device, path 3b). (b) AFM topography image (contact mode) of an imprinted array of P(VDF-TrFE) nanodots of *ca.* 85 nm height, after having filled the grooves by P3HT (spin-coating followed by annealing in toluene vapors). The left bright band corresponds to a region which was not imprinted. (c) Current-sensing AFM image of the same region, showing the current passing through the semiconducting channels separating the ferroelectric nanodots. The voltage on the bottom silver electrode was 6 V.

typically made from bistable materials exhibiting hysteresis in one of their properties.[3,4] Among bistable organic materials, ferroelectric polymers such as the copolymers of the poly(vinylidene fluoride) family are especially suited for nonvolatile storage since they exhibit a permanent polarization whose direction can be switched by the application of an electric field.[5−7] Until recently, ferroelectric polymers were typically used in capacitive memories or as gate dielectrics in ferroelectric field-effect transistors.[8]

In 2008, Asadi *et al.*[9] showed that phase-separated blends of a ferroelectric and of a semiconducting polymer could be used to fabricate a functional layer combining both storage and reading capabilities. The storage capability is provided by the ferroelectric component, with bits 1 and 0 being associated with the two opposite directions of the electrical polarization; the reading capability is provided by semiconducting channels connecting top to bottom electrodes. The current flowing through the semiconductor channels is modulated by the permanent polarization state of the nearby ferroelectric polymer, due to the bending of the semiconductor bands by the stray field of the ferroelectric material at the electrode interfaces, as discussed extensively elsewhere.[9−12] For large enough injection barriers at the semiconductor/electrode interface, the stray field of the poled ferroelectrics can indeed modulate the height of the injection barrier and switch the charge injection regime from injection-limited to space-charge-limited, depending on the direction of the polarization of the ferroelectrics. Compared to ferroelectric capacitance or transistor memories, these two-terminal dual-component diodes present significant advantages in terms of scalability, ease of integration, and reduction of cross-talks in integrated memory arrays.[11]

However, the random character of the phase separation process between the two polymer components leads to memory layers that are limited in integration density due to the irregular and coarse distribution of the semiconducting channels in the ferroelectric continuous layer. Controlling the morphology of phase-separated blends in order to achieve high storage densities remains a significant challenge.[13] Therefore, we developed a new designing concept for the bifunctional layer and applied it to this specific device in order to increase considerably the range of accessible storage densities. Our top-down design strategy consists of first creating a regular array of ferroelectric nanodots by nanoimprint lithography, followed by the filling of the trenches separating the ferroelectric nanodots with a semiconducting polymer (Figure 1a). We demonstrate the modulation of the current in the semiconductor by the polarization state of the ferroelectric material, both at the scale of a single semiconductor channel and in a microscopic device measuring about 80 000 channels in parallel. Given a channel size in the range of 150 nm, and ferroelectric nanodots of about 250 nm side, the device has a theoretical storage density of 0.2 Gb/cm^2. Importantly, in addition to shaping the layer into an array of nanodots, the nanoimprinting process also promotes a more homogeneous crystal nucleation and a preferential orientation of the crystallographic axes of the imprinted material, as was demonstrated by us and others before.[14−22] For the ferroelectric polymer, this preferential

orientation translates in decreased coercive fields,[16,22] which in the present case also results in a low voltage operation of the memory device.

RESULTS AND DISCUSSION

The structure of the diodes consists of an imprinted array of nanodots of ferroelectric poly(vinylidene fluoride-*ran*-fluoroethylene) (P(VDF-TrFE)) embedded in a continuous thin film of p-type semiconducting regioregular poly(3-hexylthiophene) (P3HT), sandwiched between two electrodes (Figure 1a). The first electrode is made of either poly(3,4-ethylenedioxythiophene): polystyrene sulfonic acid (PSS:PEDOT) or of highly boron-doped polycrystalline diamond (BdD). With work functions W_s of, respectively, ~5.1 and ~5.2 eV,[23,24] PSS:PEDOT and BdD form with P3HT ohmic contacts for hole transport since the higher occupied molecular orbital (HOMO) of P3HT is *ca.* 5.1 eV lower than the vacuum level.[25] The second electrode is made of silver; it was selected based on prior results[10] and on a preliminary study by current-sensing atomic force microscopy (CS-AFM) of different metal electrodes. Given a silver work function of 4.4−4.7 eV,[26,27] the Ag/P3HT contact is injecting for holes, with a moderate injection barrier of 0.4−0.7 eV. According to the current understanding of ferroelectric/semiconducting blend diodes,[12] the modulation of this barrier by the stray field of the poled ferroelectric material is responsible for the memory effect of the device.

Experiments were first performed on samples in which the silver electrode was at the bottom of the device, while the top electrode consisted of a movable BdD-covered AFM tip. A P(VDF-TrFE) solution was spin-coated over the silver electrode and subsequently nanoimprinted in the paraelectric liquid crystalline phase of P(VDF-TrFE) using silicon molds consisting of square cavities of lateral size l and depth d, arranged over a square lattice of period p. Different molds were used in this work; typical values of the cavity array are $p = 350$ nm, $l = 250$ nm, and $d = 200$ nm, corresponding to a surface fraction of cavities, l^2/p^2, of *ca.* 0.5. The film thickness h = ~40−50 nm was selected to ensure imprinting in complete confinement, that is, contact of the protrusions of the mold with the top of the silver electrode, which can be obtained provided $hp^2/l^2 \leq d$. As a result, the P(VDF-TrFE) film was transformed into an array of square dots of height hp^2/l^2 and lateral size l, with open trenches of width $(p - l)$ separating them; in some regions, partial tearing of the film after demolding resulted in a limited lateral displacement of the nanodots (Figure 1b). Piezoresponse force microscopy (PFM) hysteresis loops performed on continuous and imprinted samples confirmed that imprinting decreases significantly the coercive field,[16,22] with the hysteresis loop extending from −1.8 to 1.8 V for a nanoimprinted sample of *ca.* 90 nm nanodot height, compared to from −5 to 5 V for a continuous thin film of *ca.* 80 nm thickness submitted to the same annealing treatment as in NIL (Supporting Information, Figure S1).

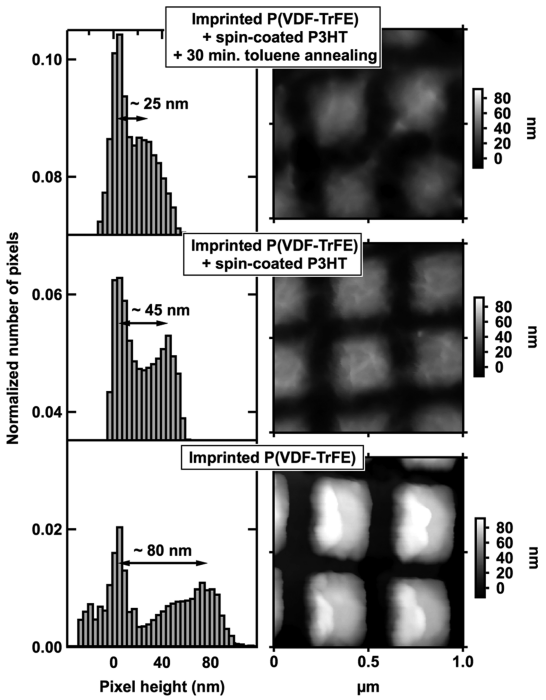

Figure 2. AFM height images (tapping mode) and related histograms of pixel height for a sample of P(VDF-TrFE) nanoimprinted over a PSS:PEDOT electrode (bottom row), a similar sample after spin-coating a layer of P3HT of 20 nm nominal thickness (middle row), and the same sample after 30 min annealing in toluene vapor (top row). The progressive smoothing of the topography is obvious. For this specific experiment, a mold of period and cavity size slightly larger than usual was used (p = *ca.* 435 nm, l = *ca.* 300 nm), keeping a similar surface fraction of cavities, in order to see better the impregnation process of the grooves.

The semiconducting polymer was then spin-coated over the imprinted array of P(VDF-TrFE) nanodots, thereby partially filling the trenches and covering the ferroelectric nanodots. It was first verified that toluene is a suitable orthogonal solvent, capable of dissolving the semiconductor polymer while leaving unaffected the imprinted P(VDF-TrFE) array (Supporting Information, Figure S2). Experiments were then performed with different spin-coating conditions. The best results were obtained when the spin-coating was performed from 1 wt % toluene solutions; for example, at 7000 rpm, films of 20 nm thickness (hereafter called the "nominal thickness") are obtained when performed over smooth substrates. When spin-coated over P(VDF-TrFE) nanodots of *ca.* 80 nm height, the difference of average height between the higher and lower points of the structure was *ca.* 45 nm after spin-coating, indicating that less P3HT accumulates over the dots than in the trenches (Figure 2). Since an optimal functioning of the device requires minimizing the layer of P3HT atop the ferroelectric nanodots and filling the trenches to as high a level as possible, the sample was annealed in toluene vapors to displace P3HT from the

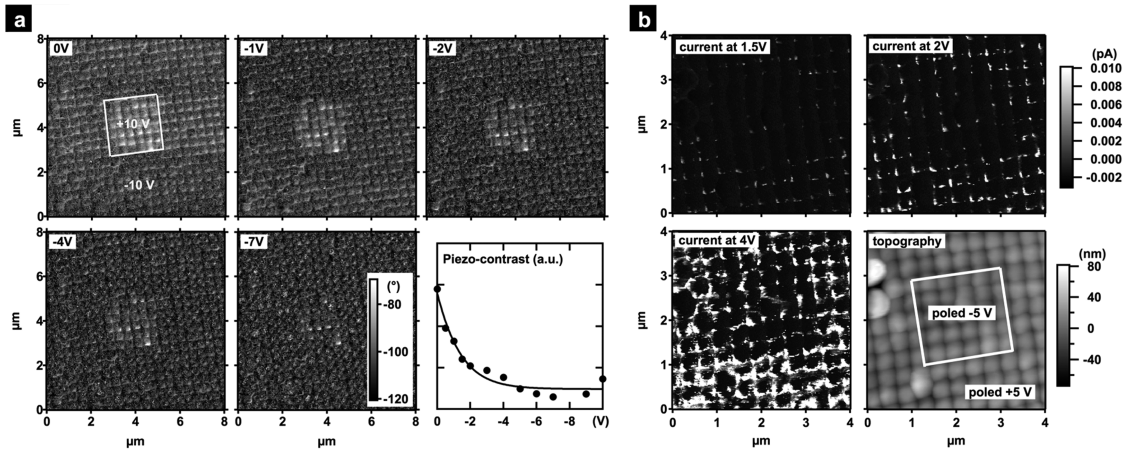

Figure 3. Local electrical characterization of a hybrid ferroelectric/semiconducting layer, made of nanoimprinted P(VDF-TrFE) nanodots of *ca.* 85 nm height separated by grooves filled with P3HT (of 15 nm nominal thickness). (a) Piezoresponse force microscopy. The sample was poled locally before measurement as shown in the top left image. The next images correspond to the PFM phase measured for different voltages applied to the bottom electrode (indicated in the images). The bottom right graph is the variation of the piezo-contrast between the positively and negatively poled regions for increasing negative voltages applied to the bottom electrode, showing the progressive reversal of the polarization. (b) Current-sensing AFM measurements of the current flowing in the layer, depending on the applied reading voltage. The sample was poled locally before measurement as shown in the bottom right AFM topography image. A modulation of the current depending on poling is observed.

top of the ferroelectric nanodots and accumulate it into the separating trenches. It should be noted that the surface tension of PVDF (considered here as close to the one of P(VDF-TrFE)) is *ca.* 30.4 mJ m^{-2},[28] while the one of P3HT is 28.6 mJ m^{-2}.[29] Using the Oss–Chaudhury–Good approach as detailed elsewhere,[30] we estimated the interfacial tension between P3HT and PVDF to be negligible, *ca.* 0.25 mJ m^{-2}, indicating that wetting of the P(VDF-TrFE) nanogrooves by the swollen P3HT should not be impossible. Annealing in toluene vapors for 30 min indeed decreased the difference of average height of the previous sample from *ca.* 45 to *ca.* 25 nm (Figure 2). This smoothing-out of the height fluctuation indicates a partial transfer of P3HT from the top of the ferroelectric nanodots to the separating grooves. At the end of the process, it is likely that a thin layer of P3HT still covers the top of the ferroelectric nanodots. Nevertheless, current-sensing (CS) AFM experiments confirmed the absence of current flowing from the bottom electrode to the top of the ferroelectric nanodots, suggesting this layer to be very thin and not continuous (Figure 1c). In addition, CS-AFM demonstrated the opening of the trenches down to the silver electrode and the successful accumulation of P3HT in them (Figure 1c), leading to current passing from the bottom silver electrode to the top (BdD-coated AFM tip) electrode.

Piezoresponse force microscopy was then performed on the hybrid semiconductor/ferroelectric layer, to check the persistence of the ferroelectric properties of P(VDF-TrFE) after processing, in the presence of the semiconductor (see Materials and Methods for details). Before the PFM measurement, the tip was first grounded, and the sample was locally poled downward by scanning the tip over a $4 \times 4\ \mu m^2$ region while applying $V_{DC} = -10$ V on the silver electrode. Then, a smaller $2 \times 2\ \mu m^2$ upward-poled region was written within the first one, using a positive electrode voltage ($V_{DC} = 10$ V). Maps of the polarization were then measured in PFM mode while applying increasingly negative voltages V_{DC} to the bottom electrode (Figure 3a). Here, the application of the static V_{DC} voltage on the bottom electrode progressively changes the direction of polarization of the central region from up to down, while simultaneously polarizing nonpermanently the whole sample. As a result, the contrast between the upward- and downward-poled regions is progressively fading when V_{DC} increases in absolute value, due to the downward-switching of the upward-poled central region. The contrast fades rapidly and is mostly lost above *ca.* 2 V (Figure 3a), demonstrating polarization switching in this low-voltage range. These experiments indicate that the ferroelectric properties of P(VDF-TrFE) are preserved in the hybrid layer, and that switching occurs at low values of voltage as found for the imprinted P(VDF-TrFE) only (Supporting Information, Figure S1). This is a further confirmation that the probable thin residual P3HT layer atop the ferroelectric nanodots is of little consequence for the functioning of the device.

The same sample was probed by current-sensing AFM, using a similar procedure. The sample was first poled upward by scanning the grounded tip over a $4 \times 4\ \mu m^2$ area, while applying $V_{DC} = +5$ V on the bottom electrode. The sample was subsequently imaged again with $V_{DC} = 0$ V to discharge possibly trapped charges. Then, the sample was poled downward within the previously poled frame, by scanning the grounded tip over a smaller $2 \times 2\ \mu m^2$ area while applying $V_{DC} = -5$ V on the silver electrode. In a final step, maps of the current flowing from the silver electrode to the grounded tip were obtained for

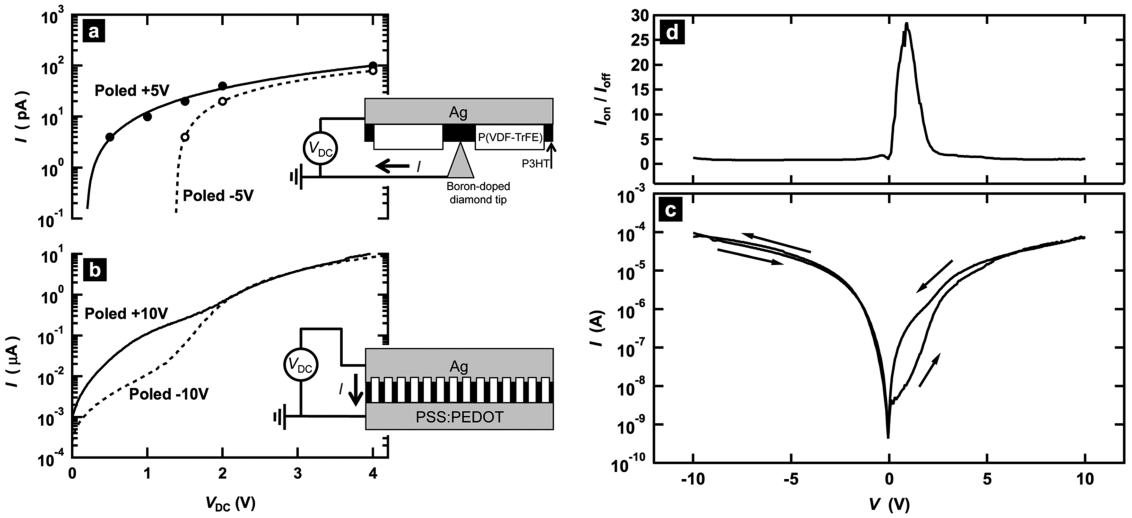

Figure 4. Hysteresis of the current flowing in a hybrid ferroelectric/semiconducting layer made of nanoimprinted P(VDF-TrFE) nanodots of *ca.* 85 nm height separated by grooves filled with P3HT (of 20 nm nominal thickness). (a,b) Comparison between the local measurement of the current flowing in the hybrid layer by CS-AFM (a), and the current flowing in a microscopic device of (100 μm)^2 cross-section (b), depending on prior poling of the area or device. In panel a, the lines are drawn to guide the eye. (c,d) Current/voltage hysteresis loop measured on a microscopic diode of (100 μm)^2 cross section (c), and ratio between the currents in the off and on states (d).

increasing positive values of V_{DC} on the silver electrode. Figure 3b shows that current is flowing in the gaps open in the P(VDF-TrFE) layer when V_{DC} is high enough. In addition, the current flowing within the upward-poled external region is on average higher than in the downward-poled central region, demonstrating the modulation of the device current depending on poling. Note that the current tends to be larger at the intersection between two grooves due to a larger area of contact of the AFM tip at these locations.

We found that the modulation of current is depending on the nominal thickness of the P3HT spin-coated layer (d_{P3HT} = 10, 15, and 20 nm). This might be due in part to the dependence of the current on the contact area between tip and sample, which may be limited in the recesses of the layer; the height of P3HT in the grooves and the amount of residual P3HT on the top of the ferroelectric nanodots are supplementary factors. The stronger current modulation was observed for 20 nm P3HT nominal thickness. Larger nominal thicknesses were not investigated, as they correspond to thicker P3HT layers on the ferroelectric nanodots which is likely to be detrimental for operation. Figure 4a presents for this specific sample the current flowing from bottom to top electrode, depending on reading voltage (V_{DC}), for upward- and downward-poled regions (the tip was positioned at the intersection of two P3HT-filled grooves, which corresponds to a vertical semiconducting channel of about 140 nm diagonal length). A strong modulation of the current depending on the polarization of the P(VDF-TrFE) layer is observed when V_{DC} is below *ca.* 2 V, with the ratio of on-to-off currents (I_{on}/I_{off}) being 5 at V_{DC} = 1.5 V, or even larger for lower V_{DC}. The loss of modulation above 2 V is consistent with the PFM results which indicated that the polarization switching is essentially done at 2 V.

Increasing the switching to higher voltages requires increasing the thickness of the P(VDF-TrFE) layer. However, attempts to do so were unsuccessful because thicker layers resulted in stronger adhesion to the molds and therefore very defective samples. A similar experiment was performed, using poly(triarylamine) (PTAA) instead of P3HT. In this case, a poling voltage of $\pm$10 V was used, and the current flowing from the silver electrode to tip was measured at a reading voltage of 1 V; the on and off currents were 30 and $\sim$0 pA, respectively, showing that the device could also work with another semiconducting polymer having a similar HOMO level (*ca.* 5.0$-$5.2 eV).[31,32]

A hybrid P3HT/P(VDF-TrFE) microscopic device was also realized and compared to the previous measurements, in order to obtain the collective behavior of a series of semiconducting channels. In addition, because such a large device is much more sensitive to defects in the layer, this test also serves to evaluate the general quality of the fabrication process of the hybrid layer. Here, a gold line of 100 μm width and 50 nm thickness was first deposited, followed by spin-coating of a PSS:PEDOT layer of 100 nm thickness. A P(VDF-TrFE) layer was then deposited and imprinted as described before. The imprinting process is self-aligned: because the bottom electrode protrudes by 150 nm over the rest of the substrate, the P(VDF-TrFE) is properly imprinted over the electrode only. After P3HT spin-coating, a crossed top Ag electrode of 100 μm width was evaporated through a shadow mask. The PSS:PEDOT electrode was grounded, and the ferroelectric polymer was poled downward (upward) by applying V_{DC} = +10 V ($-$10 V) on the top Ag electrode. Then, the current

flowing in the device was measured for increasing positive values of V_{DC} (Figure 4b). Again, the current I_{on} flowing in the device was significantly larger when the polarization of the ferroelectric nanodots was pointing away from the Ag electrode, compared to the current I_{off} when the polarization of the nanodots was pointing toward the Ag electrode. Most importantly, the 0−2 V memory window on the device of 100 μm^2 cross section (Figure 4b), which comprises *ca.* 80 000 ferroelectric nanodots, compares well with the local measurements performed on a single current channel by CS-AFM (Figure 4a). It is more difficult to compare precisely the current levels since defects might exist in the microscopic device and since the exact contact surface is unknown in the case of the local CS-AFM experiment. Nevertheless, the factor of $\sim 10^4$ between the current levels measured at 1 V in the macroscopic and local measurements is in the expected range because the microscopic device comprises a few tens of thousands of cells. This demonstrates that our fabrication process can lead to layers of good quality over 100 μm^2. The Supporting Information provides another proof that hybrid layers of good quality can be obtained by our process over large areas, using a range of materials and different shaping geometries: in the specific case of Figure S3, the electrode size is as large as 1 cm^2, while the hybrid layer consists of an array of parallel P(VDF-TrFE) imprinted lines of 65 nm width interspersed with (P3HT/PCBM) semiconducting polymer blend.

Figure 4c is the complete hysteresis curve of the current flowing in the microscopic device when the voltage is swept from −10 V to +10 V and back. Since the bottom PSS:PEDOT electrode provides an ohmic contact with P3HT, no modulation of current is observed on the negative reading voltage side, as expected. The ratio between the currents, which is the on/off ratio, is displayed in Figure 4d, showing that in the positive reading voltage region values as high as 25 can be obtained. Further increases of this on/off ratio should be possible by improving the design of the device, tuning the electrode/semiconductor interface, and decreasing the number of defects after imprinting.

CONCLUSIONS

Our results demonstrate the possibility to design a multifunctional organic layer of large area by rationally combining nanosized regions of different functional polymers. The proposed methodology involves shaping a first component by nanoimprinting, followed by the filling of open spaces by the second component. Instead of relying on a spontaneous and random phase separation process, or on the tedious synthesis of block copolymers, the method allows one to tailor a hybrid active layer in order to combine synergetically orthogonal functional properties with a fine control over their spatial distribution. In this respect, despite the numerous technological improvements certainly remaining to be made in the future, our methodology offers an unprecedented way to fabricate sophisticated multifunctional organic layers for a range of possible applications. Most importantly, it could be easily generalized to other types of hybrid multifunctional layers such as, for example, found in solar cells[33,34] or multiferroic composite materials.

Concerning the specifically targeted application of this article, we note that, compared to the previously reported phase-separated blend memory diodes, imprinted diodes have the advantage to display a regular hybrid structure of semiconducting and ferroelectric regions of very small size, with increased storage densities being thus possible. CS-AFM results show that a single storage cell could be limited to four ferroelectric nanodots separated by two crossed channels of semiconductor, corresponding to a footprint of 700 × 700 nm^2. However, to fully exploit this value, further technological work will be needed to deposit aligned electrode strips of appropriate width. The storage density could thus potentially be as high as *ca.* 0.2 Gb/cm^2 and increased scaling down of the ferroelectric nanodots—which is not forbidden by fundamental principles[35−38]—would increase further this value. With P3HT as semiconductor, the typical current flowing in such a small device is on the order of a few tens of pA; higher currents could be obtained with semiconductors of higher mobility or by improving the postprocessing treatment of P3HT. Alternatively, one can compromise storage density and increase the current density, by making larger devices comprising many such cells sandwiched in parallel between two crossed electrodes. Then, currents in the range of μA can be obtained for electrode sizes in the 100 μm range (~64 kb/in^2). In this case, however, it is of utmost importance to improve the quality of the imprinting process because defects add up in parallel. A second advantage resulting from imprinting is the low switching voltage, which is of interest for low-power operation. The switching voltage of our device is *ca.* 2 V, corresponding to fields of *ca.* 25 MV/m. This low value is the result of the limited thickness of the ferroelectric dots, combined with the beneficial effect of nanoimprinting which reduces the coercive field of P(VDF-TrFE) as we demonstrated before.[16,22]

MATERIALS AND METHODS

Materials and Processes. P(VDF-TrFE) was obtained from Solvay Specialty Polymers (30 wt % of TrFE units; weight-average molar mass *ca.* 340 000). Regioregular poly(3-hexylthiophene) (P3HT) was purchased from Aldrich. P(VDF-TrFE) was dissolved in cyclohexanone (25 g/L) and was spin-coated over the bottom

electrode, leading typically to a film thickness of ~40−50 nm for a spin-coating speed of 6000 rpm. The bottom electrode was either a 100 nm thick Ag electrode deposited by thermal evaporation or a 100 nm thick PSS:PEDOT electrode spin-coated over a 50 nm thick layer of evaporated gold. In both cases, the bottom electrode was deposited on a silicon wafer covered by a thick layer of insulating oxide. The ferroelectric film was subsequently imprinted with an Obducat imprinter in the paraelectric liquid crystalline phase of P(VDF-TrFE) for 10 min at 135 °C and 60 bar, then cooled to room temperature. The molds were prepared by electron beam lithography and were coated with a monolayer of perfluorodecyldimethylchlorosilane (Gelest) for decreased adhesion.

Piezoresponse Force Microscopy and Current-Sensing AFM. Experiments were performed with an Agilent 5500 microscope equipped with a Mac III triple lock-in amplifier (Agilent), using Si cantilevers of 0.5 N/m nominal bending rigidity, coated with boron-doped diamond (CDT-CONTR from Nanosensors). For CS-AFM, the tip was grounded and the DC bias was applied to the bottom electrode. For PFM, the tip was additionally submitted to a small alternative voltage $V_{AC} = V_0\cos(\omega t)$ ($V_0 = 0.5$ V and $\omega \sim 565 \times 10^3$ s^{-1} close to the resonance frequency of the tip when in contact with the sample). Due to the converse piezoelectric effect, the alternating electric field generates an oscillating deformation of the sample in the direction perpendicular to the electric field, $A(t) = A\cos(\omega t + \phi)$, which is detected by the vertical deflection of the cantilever having its tip in contact with the sample.[39] The PFM amplitude (A) is proportional to the absolute value of the converse piezoelectric coefficient, which is itself related to the permanent polarization of the sample. The phase signal (ϕ), which indicates the phase difference between the mechanical oscillation and the electric voltage applied to the tip, should be either 0 or 180° depending on whether the average dipole moment points down or up, respectively. However, due to the existence of other sources of electromechanical coupling, the measured phase angles are often different from these expected values.[39] The contrast between the two differently poled regions was defined as $(1/2) \times (A^+\cos(\phi^+) - A^-\cos(\phi^-))$, where the superscripts "+" and "−" refer to the direction of the polarization (+ = upward).

Conflict of Interest: The authors declare no competing financial interest.

Acknowledgment. Financial support was provided by the EU Program FP7/2007-2013 (MOMA, agreement no. 248092), the Belgian Federal Science Policy (IAP P7/05), and the F.R.S.-FNRS. The authors thank N. Afsharimani and D. Magnin for technical help.

Supporting Information Available: PFM hysteresis loops of a continuous film and a nanoimprinted array of P(VDF-TrFE); effect of toluene on an imprinted array of P(VDF-TrFE); current/voltage curve of a nanoimprinted P(VDF-TrFE)/(P3HT:PCBM) hybrid layer probed over 1 cm^2. This material is available free of charge *via* the Internet at http://pubs.acs.org.

REFERENCES AND NOTES

1. Isayev, A. I. Encyclopedia of Polymer Blends, Volume 1: Fundamentals. Wiley-VCH: Weinheim, Germany, 2010.
2. Schacher, F. H.; Rupar, P. A.; Manners, I. Functional Block Copolymers: Nanostructured Materials with Emerging Applications. *Angew. Chem., Int. Ed.* **2012**, *51*, 7898–7921.
3. Ling, Q.-D.; Liaw, D.-J.; Zhu, C.; Chan, D. S.-H.; Kang, E.-T.; Neoh, K.-G. Polymer Electronic Memories: Materials, Devices and Mechanisms. *Prog. Polym. Sci.* **2008**, *33*, 917–978.
4. Heremans, P.; Gelinck, G. H.; Müller, R.; Baeg, K.-J.; Kim, D.-Y.; Noh, Y.-Y. Polymer and Organic Nonvolatile Memory Devices. *Chem. Mater.* **2011**, *23*, 341–358.
5. Lovinger, A. J. Ferroelectric Polymers. *Science* **1983**, *220*, 1115–1121.
6. Furukawa, T. Ferroelectric Properties of Vinylidene Fluoride Copolymers. *Phase Transitions* **1989**, *18*, 143–211.
7. Balta Calleja, F. J.; Arche, A. G.; Ezquerra, T. A.; Santa Cruz, C.; Batallan, F.; Frick, B.; Cabarcos, E. L. Structure and Properties of Ferroelectric Copolymers of Poly(vinylidene fluoride). *Adv. Polym. Sci.* **1993**, *108*, 1–48.
8. Naber, R. C. G.; Asadi, K.; Blom, P. W. M.; de Leeuw, D. M.; de Boer, B. Organic Nonvolatile Memory Devices Based on Ferroelectricity. *Adv. Mater.* **2009**, *22*, 933–945.
9. Asadi, K.; de Leeuw, D. M.; de Boer, B.; Blom, P. W. M. Organic Non-volatile Memories from Ferroelectric Phase-Separated Blends. *Nat. Mater.* **2008**, *7*, 547–550.
10. Asadi, K.; de Boer, T. G.; Blom, P. W. M.; de Leeuw, D. M. Tunable Injection Barrier in Organic Resistive Switches Based on Phase-Separated Ferroelectric-Semiconductor Blends. *Adv. Funct. Mater.* **2009**, *19*, 3173–3178.
11. Asadi, K.; Li, M.; Blom, P. W. M.; Kemerink, M.; de Leeuw, D. M. Organic Ferroelectric Opto-electronic Memories. *Mater. Today* **2011**, *14*, 592–599.
12. Kemerink, M.; Asadi, K.; Blom, P. W. M.; de Leeuw, D. M. The Operational Mechanism of Ferroelectric-Driven Organic Resistive Switches. *Org. Electron.* **2012**, *13*, 147–152.
13. Li, M.; Stingelin, N.; Michels, J. J.; Spijkman, M.-J.; Asadi, K.; Beerends, R.; Biscarini, F.; Blom, P. W. M.; de Leeuw, D. M. Processing and Low Voltage Switching of Organic Ferroelectric Phase-Separated Bistable Diodes. *Adv. Funct. Mater.* **2012**, *22*, 2750–2757.
14. Hu, Z.; Baralia, G.; Bayot, V.; Gohy, J. F.; Jonas, A. M. Nanoscale Control of Polymer Crystallization by Nanoimprint Lithography. *Nano Lett.* **2005**, *5*, 1738–1743.
15. Hu, Z.; Muls, B.; Gence, L.; Serban, D. A.; Hofkens, J.; Melinte, S.; Nysten, B.; Demoustier-Champagne, S.; Jonas, A. M. High-Throughput Fabrication of Organic Nanowire Devices with Preferential Internal Alignment and Improved Performance. *Nano Lett.* **2007**, *7*, 3639–3644.
16. Hu, Z.; Tian, M.; Nysten, B.; Jonas, A. M. Regular Arrays of Highly Ordered Ferroelectric Polymer Nanostructures for Non-volatile Low-Voltage Memories. *Nat. Mater.* **2009**, *8*, 62–67.
17. Hu, Z.; Jonas, A. M. Control of Crystal Orientation in Soft Nanostructures by Nanoimprint Lithography. *Soft Matter* **2010**, *6*, 21–28.
18. Liu, Y.; Weiss, D. N.; Li, J. Rapid Nanoimprinting and Excellent Piezoresponse of Polymeric Ferroelectric Nanostructures. *ACS Nano* **2010**, *4*, 83–90.
19. Fang, J.-R.; Luo, X.-Y.; Ma, Z.; Shen, Z.-K.; Lu, Q.; Lu, B.-R.; Zhu, G.-D.; Qu, X.-P.; Liu, R.; Chen, Y.-F. Influence of Nanoembossing on Properties of Poly(VDF-TrFE). *Microelectron. Eng.* **2010**, *87*, 890–892.
20. Fang, J.-R.; Shen, Z.-K.; Yang, S.; Lu, Q.; Li, J.; Chen, Y.-F.; Liu, R. Nanoimprint of Ordered Ferro/Piezoelectric P(VDF-TrFE) Nanostructures. *Microelectron. Eng.* **2011**, *88*, 2033–2036.
21. Martínez-Tong, D. E.; Soccio, M.; García-Gutiérrez, M. C.; Nogales, A.; Rueda, D. R.; Alayo, N.; Pérez-Murano, F.; Ezquerra, T. A. Improving Information Density in Ferroelectric Polymer Films by Using Nanoimprinted Gratings. *Appl. Phys. Lett.* **2013**, *102*, 191601.
22. Kassa, H. G.; Cai, R.; Marrani, A.; Nysten, B.; Hu, Z.; Jonas, A. M. Structure and Ferroelectric Properties of Nanoimprinted Poly(vinylidene fluoride-*ran*-trifluoroethylene). *Macromolecules* **2013**, *46*, 8569–8579.
23. Liu, K.; Zhang, B.; Wan, M.; Chu, J. H.; Johnston, C.; Roth, S. Measurement of Electron Affinity in Boron-Doped Diamond From Capacitance Spectroscopy. *Appl. Phys. Lett.* **1997**, *70*, 2891–2893.
24. Nardes, A. M.; Kemerink, M.; de Kok, M. M.; Vinken, E.; Maturova, K.; Janssen, R. A. J. Conductivity, Work Function, and Environmental Stability of PEDOT:PSS Thin Films Treated with Sorbitol. *Org. Electron.* **2008**, *9*, 727–734.
25. Dediu, V. A.; Hueso, L. E.; Bergenti, I.; Taliani, C. Spin Routes in Organic Semiconductors. *Nat. Mater.* **2009**, *8*, 707–716.
26. de Boer, B.; Hadipour, A.; Mandoc, M. M.; van Woudenbergh, T.; Blom, P. W. M. Tuning of Metal Work Functions with Self-Assembled Monolayers. *Adv. Mater.* **2005**, *17*, 621–625.
27. Hong, J.-P.; Park, A.-Y.; Lee, S.; Kang, J.; Shin, N.; Yoon, D. Y. Tuning of Ag Work Functions by Self-Assembled Monolayers of Aromatic Thiols for an Efficient Hole Injection for Solution Processed Triisopropylsilylethynyl Pentacene

Organic Thin Film Transistors. *Appl. Phys. Lett.* **2008**, *92*, 143311.
28. Morra, M.; Della Volpe, C.; Siboni, S. The Evaluation of Acid−Base Properties of Polymer Surfaces by Wettability Measurements. In *Polymer Interfaces and Emulsions*; Esumi, K., Ed.; Marcel Dekker: New York, 1999; pp 535−566.
29. Li Destri, G.; Keller, T. F.; Catellani, M.; Punzo, F.; Jandt, K. D.; Marletta, G. Crystalline Monolayer Ordering at Substrate/Polymer Interfaces in Poly(3-hexylthiophene) Ultrathin Films. *Macromol. Chem. Phys.* **2011**, *212*, 905–914.
30. Baralia, G. G.; Filiâtre, C.; Nysten, B.; Jonas, A. M. Nanodecoding by Dewetting. *Adv. Mater.* **2007**, *19*, 4453–4459.
31. Thelakkat, M. Star-Shaped, Dendrimeric and Polymeric Triarylamines as Photoconductors and Hole Transport Materials for Electro-optical Applications. *Macromol. Mater. Eng.* **2002**, *287*, 442–461.
32. Kroeze, J. E.; Hirata, N.; Schmidt-Mende, L.; Orizu, C.; Ogier, S. D.; Carr, K.; Grätzel, M.; Durrant, J. R. Parameters Influencing Charge Separation in Solid-State Dye-Sensitized Solar Cells Using Novel Hole Conductors. *Adv. Funct. Mater.* **2006**, *16*, 1832–1838.
33. Yuan, Y.; Reece, T. J.; Sharma, P.; Poddar, S.; Ducharme, S.; Gruverman, A.; Yang, Y.; Huang, J. Efficiency Enhancement in Organic Solar Cells with Ferroelectric Polymers. *Nat. Mater.* **2011**, *10*, 296–302.
34. Yang, Y.; Mielczarek, K.; Aryal, M.; Zakhidov, A.; Hu, W. Nanoimprinted Polymer Solar Cell. *ACS Nano* **2012**, *6*, 2877–2892.
35. Bune, A. V.; Fridkin, V. M.; Ducharme, S.; Blinov, L. M.; Palto, S. P.; Sorokin, A. V.; Yudin, S. G.; Zlatkin, A. Two-Dimensional Ferroelectric Films. *Nature* **1998**, *391*, 874–877.
36. Lutkenhaus, J. L.; McEnnis, K.; Serghei, A.; Russell, T. P. Confinement Effects on Crystallization and Curie Transitions of Poly(vinylidene fluoride-*co*-trifluoroethylene). *Macromolecules* **2010**, *43*, 3844–3850.
37. Serghei, A.; Lutkenhaus, J. L.; Miranda, D. F.; McEnnis, K.; Kremer, F.; Russell, T. P. Density Fluctuations and Phase Transitions of Ferroelectric Polymer Nanowires. *Small* **2010**, *6*, 1822–1826.
38. Serghei, A.; Zhao, W.; Miranda, D.; Russell, T. P. Curie Transitions for Attograms of Ferroelectric Polymers. *Nano Lett.* **2013**, *13*, 577–580.
39. Kalinin, S. V.; Rar, A.; Jesse, S. A Decade of Piezoresponse Force Microscopy: Progress, Challenges, and Opportunities. *IEEE Trans. Ultrason. Ferroelectr. Freq. Control* **2006**, *53*, 2226–2252.